AAS 15-299

OPTIMIZED LOW-TRUST MISSION TO THE ATIRA ASTEROIDS

Marilena Di Carlo[*], Natalia Ortiz Gómez[†], Juan Manuel Romero Martín[*], Chiara Tardioli[*], Fabien Gachet[‡], Kartik Kumar[§] and Massimilano Vasile[¶]

Atira asteroids are recently-discovered celestial bodies characterized by orbits lying completely inside the Earth's. The study of these objects is difficult due to the limitations of ground-based observations: objects can only be detected when the Sun is not in the field of view of the telescope. However, many asteroids are expected to exist in the inner region of the Solar System, many of which could pose a significant threat to our planet. In this paper, a mission to improve knowledge of the known Atira asteroids in terms of ephemerides and composition and to observe inner-Earth asteroids is presented. The mission is realized using electric propulsion, which in recent years has proven to be a viable option for interplanetary flight. The trajectory is optimized in such a way as to visit the maximum possible number of asteroids of the Atira group with the minimum propellant consumption; the mission ends with a transfer to an orbit with perigee equal to Venus's orbit radius, to maximize the observations of asteroids in the inner part of the Solar System.

INTRODUCTION

Atira asteroids are Near-Earth Asteroids (NEAs) with both perihelion and aphelion within the orbit of the Earth (semimajor axis $a < 1$ AU and aphelion $Q < 0.983$ AU), also called Inner-Earth Objects (IEOs). The first Atira object was discovered in 2003 and, as of December 2014, only fourteen asteroids are counted in this group (Table 1), [1]. However, many more objects are expected to exist in the same region of the Solar System. To date, over eleven thousand NEAs have been identified, the majority of which are characterized by a semimajor axis greater than 1 AU, as shown in Figure 1, where the distribution of the known NEAs is shown in the $a - e$ and $a - i$ planes, with the Atira asteroids represented in red. Inner Solar System asteroids are indeed difficult to detect because of the limitations of ground-based survey: telescopes can only search on the night side of the Earth, where the Sun is not in the field of view. For this reason these asteroids could represent a hazard for our planet. For example, the object that exploded in an air burst over Chelyabinsk, in Russia, in February 2013, injuring more than 1,000 people, approached, undetected, from the Sun direction.

In recent years, successful missions such as Deep Space 1 [2], Hayabusa [3] and Dawn [4] - which is currently en route to Ceres, the largest object in the asteroid belt - have demonstrated the possibility to successfully survey or even land on asteroids in our Solar System. However, to date no mission has targeted inner Solar System asteroids, including members of the Atira group. The aforementioned missions make use of highly-efficient electric propulsion system, for which it has been proven the potential to result in shorter flight times, smaller launch vehicles and increased mass delivered to destination, when compared to high-thrust propulsion systems [5], [6].

This paper proposes a mission to visit the Atira asteroids, making use of an electric propulsion system. To maximize the scientific return of the spacecraft, the mission is optimized to visit the maximum possible number of asteroids of the Atira group while conducting a visibility analysis during the mission lifetime to search for new Near-Earth asteroids.

[*]PhD Student at University of Strathclyde, Glasgow, United Kingdom.
[†]PhD Student at University of Southampton, United Kingdom.
[‡]PhD Student at University of Roma Tor Vergata, Rome, Italy.
[§]Senior Engineer at Dinamica Srl, Italy.
[¶]Professor at University of Strathclyde, United Kingdom.

Table 1. Osculating orbital elements of Atira asteroids: semi-major axis (a), eccentricity (e), inclination (i), longitude of the ascending node (Ω), argument of perigee (ω), mean anomaly (M) and time of passage at perihelion (t_p), [1].

	Asteroid ID	a [AU]	e	i [deg]	Ω [deg]	ω [deg]	M [deg]	t_p [ET]
1	2003 CP20	0.7411	0.3222	25.62	103.92	252.93	336.80	2014-Dec-24.0
2	2004 XZ130	0.6176	0.4545	2.95	211.41	5.16	23.25	2014-Nov-27.6
3	2005 TG45	0.6815	0.3724	23.33	273.46	230.42	324.97	2014-Dec-29.0
4	1998 DK36	0.6923	0.4160	2.02	151.46	180.04	183.25	1998-Jun-07.3
5	2004 JG6	0.6352	0.5311	18.94	37.04	352.98	168.72	2014-Sep-13.3
6	2006 WE4	0.7847	0.1829	24.77	311.04	318.62	44.70	2014-Nov-07.5
7	2007 EB26	0.5476	0.7887	8.49	63.22	236.71	237.91	2007-Apr-30.2
8	2008 EA32	0.6159	0.3049	28.27	100.97	181.85	216.53	2015-Feb-17.4
9	2008 UL90	0.6948	0.3802	24.31	81.17	183.61	358.46	2014-Dec-09.9
10	2010 XB11	0.618	0.5338	29.88	96.32	202.48	223.70	2015-Feb-14.2
11	2012 VE46	0.7128	0.3615	6.67	8.95	190.36	8.52	2014-Dec-03.8
12	2013 JX28	0.6008	0.5641	10.76	39.97	354.88	311.78	2014-Dec-31.8
13	2013 TQ5	0.7739	0.1554	16.38	286.77	247.32	83.30	2014-Oct-12.5
14	2014 FO47	0.7524	0.2708	19.18	358.68	347.41	225.84	2015-Mar-07.8

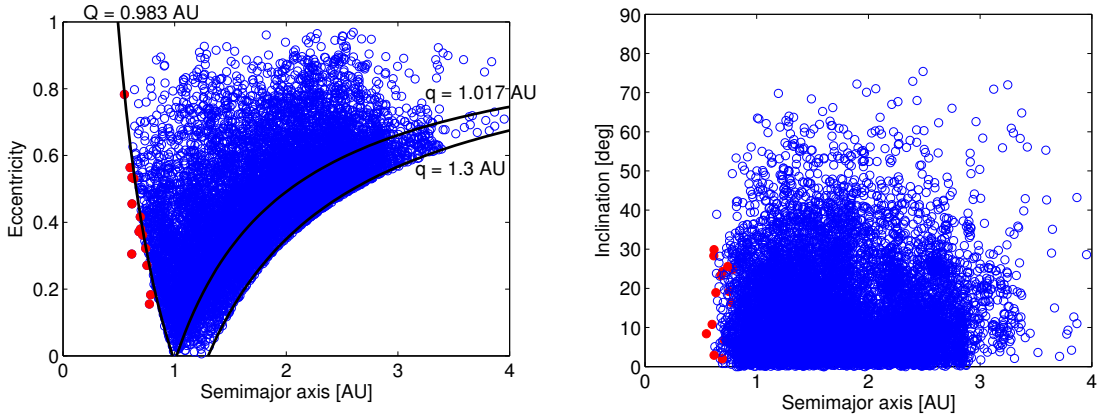

Figure 1. NEAs distribution - red circles indicate Atira asteroids (data from Minor Planet Center [7]).

MISSION DESCRIPTION

In this paper, the encounters with the Atira asteroids are designed through a series of fly-bys at the nodal points of the asteroids, using a low-thrust propulsion system.

The mission analysis was divided into three phases: 1) identification of the optimal asteroid sequence and the optimal departure and arrival dates; 2) refinement of the optimal solution using a Differential Evolution-based algorithm; 3) low-thrust trajectory optimization. Subsequently, a visibility analysis was carried out in order to assess the number of new asteroids that could potentially be observed by the spacecraft.

During the first step, a branch and prune procedure was applied to find the optimal solution, that is, the impulsive trajectory which has the minimum ΔV to realize the transfer and therefore the minimum propellant consumption. This first step involved searching over a wide range of parameters: Earth departure date, asteroids sequence, arrival dates at each of the asteroids [8]. In this phase of the mission analysis, the transfer trajectories between asteroids were modelled using the patched conic approximation and defining the trajectory as a sequence of Lambert arcs, [9], [10].

During the second step, the optimal sequence obtained by the previous analysis was further optimized using the Adaptive Inflationary Differential Evolution Algorithm [11], an adaptive stochastic optimizer which combines Differential Evolution [12] with Monotonic Basin Hopping [13]. This further optimization was done in order to identify better conditions for the departure dates, leading to a reduced ΔV for the mission.

During the last step, for the optimized set of variables previously identified, the optimal low-thrust control history for the spacecraft was determined. In particular, the control parameters of the low-thrust optimized in this phase were the thrust direction and the nodes defining the On/Off conditions for the firing of the thruster. No throttling of the propulsion system was considered.

After the last fly-by, the spacecraft was moved to a parking orbit with perigee equal to Venus's orbit semi-major axis, to allow the spacecraft to continue its visibility survey of to the inner region of the Solar System.

SEQUENCE FINDER

Due to the complexity of optimizing low-thrust missions and handling a large design space, an optimization method based on impulsive transfers was used as initial step for the target low-thrust optimized trajectory. This optimization method spans the whole search space domain in order to find all the sub-optimal values for the design variables (departure dates, sequence of asteroids, time of flight, etc.) used in the next phase for the low-thrust optimization.

In order to find all the optimal solutions, the algorithm LambTAN (Lambert to Target Asteroids at Nodal points) was developed. This algorithm was inspired by the combination of the Branch-And-Prune and the incremental pruning proposed in [14] and [15]. Incremental pruning is based on the idea of constructing sets of trajectories, one arc at a time; the arcs are therefore independent, allowing to prune out full transfer subsets that do not satisfy a given criterion e.g., the ΔV of the arc is greater than a given maximum value. By constructing and assessing the arcs one after the other, the space of acceptable transfers is pruned out incrementally in such a way that the computational complexity is now polynomial with respect to the number of arcs. The solutions are composed adding branches and nodes incrementally with the iteration of the algorithm.

The trajectory model used in this study was based on a Lambert linked-conic trajectory. The asteroids were assumed to move on Keplerian orbits as a solution of the two-body problem Sun-Asteroid. The trajectories were composed of sequences of conic arcs linked together through discrete, instantaneous events. Each conic arc was the solution of a Lambert problem, which was solved to compute the ΔV required for the transfer to reach each asteroid at its nodal point (point defined by the intersection of the asteroid's orbit with the ecliptic plane). The arrival conditions were defined by the passage of the asteroids through their nodal points and the departure conditions were identified, on the departure orbit, by a minimum and maximum value for the time of flight to reach the nodal point. In Figure 2 is shown a schematic representation of the Lambert arcs that reach a given asteroids from different departure conditions on Earth's orbit.

Additionally, the search space was pruned in order to exclude non-feasible solutions for the low-thrust optimization by applying the Edelbaum condition for low-thrust transfer [16], as well as considering constraints for the maximum local departure ΔV, the minimum and maximum local time of flights and the minimum perihelion.

Algorithm Definition

In this subsection a description of the LambTAN algorithm is given. The algorithm starts from a given departure orbit, identified by its orbital elements, $\mathfrak{T} = \{a, e, i, \Omega, \omega\}$, where a is the semimajor axis, e is the eccentricity, i is the inclination, Ω is the right ascension of the ascending node and ω is the argument of the perihelion. For the given set of target asteroids $S = \{A_1, A_2, ..., A_d\}$, the ascending ($\Omega_{A_k}$) and descending ($\mathfrak{V}_{A_k}$) nodal points are computed for each target asteroid A_k with $k = 1, \ldots, d$. Then, the passing epochs T_{A_k} are computed, for the current selected target asteroid and for both nodal points, within the interval of time going from the considered epoch, $T_{current}$ to the end of the mission, T_{end}. For each passing epoch, a local departure window can be computed. In particular, the start (T^{LW}_{start}) and end (T^{LW}_{end}) epochs for the local

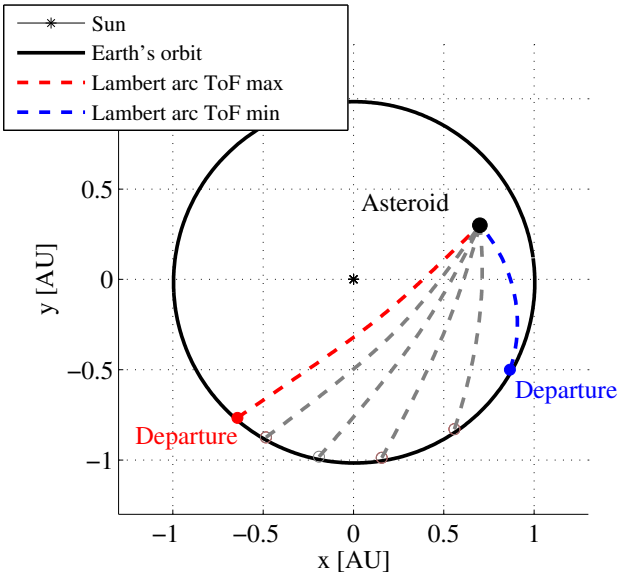

Figure 2. Lambert arcs for Earth-to-asteroid transfer example. The asteroid fly-by occurs at the nodal point. Subsequent asteroid-to-asteroid transfers were computed in analogous fashion.

departure window are computed by subtracting ToF_{min} and ToF_{max} from each computed passing epoch T_{A_k}:

$$\begin{aligned} T_{start}^{LW} &= T_{A_k} - ToF_{max}, \\ T_{end}^{LW} &= T_{A_k} - ToF_{min}. \end{aligned} \tag{1}$$

The next step is to compute, from the local departure window, n Lambert arcs that connect the departure orbit with the nodal point at the considered passing epoch, where n is given by:

$$n = \lfloor \frac{T_{end}^{LW} - T_{start}^{LW}}{ToF_{step}} \rfloor. \tag{2}$$

For a given Lambert arc, the algorithm proceeds to the next step only if three constraint criteria are met:

- the ΔV of the current Lambert arc, ΔV_{arc_k}, has to be equal or lower than a given maximum value, ΔV_{max}, due to the limitations of the maximum ΔV that can be obtained using a chemical propulsion system:

$$\Delta V_{arc_k} \leq \Delta V_{max}; \tag{3}$$

- orbits too close to the Sun are rejected; the Lambert transfer has to be characterized by a perihelion q greater than a given minimum perihelion, q_{min}:

$$q > q_{min}; \tag{4}$$

- the third constraint criterion is related to the feasibility of translating the impulsive Lambert transfer to a low-thrust transfer. The Edelbaum condition for low-thrust transfer between circular orbit was considered [16]:

$$\Delta V_{Ed} = \sqrt{V_0^2 - 2V_f V_0 \cos\left(\frac{\pi}{2}\Delta i\right) + V_f^2}. \tag{5}$$

In the previous equation, ΔV_{Ed} is the change in velocity required by the low-thrust engine to go from a departure orbit characterized by initial velocity V_0 to an orbit characterized by velocity V_f (in this case V_f is the velocity at the end of the Lambert arc, since a fly-by is considered). The incination change Δi is zero because the asteroids are targeted at the nodal points. The transfer is feasible using the Edelbaum condition if:

$$ToF_{arc_k}\epsilon \geq \Delta V_{Ed}, \tag{6}$$

where ToF_{arc_k} is the time of flight for the current Lambert arc and ϵ is the acceleration provided by the low-thrust engine. Although Edelbaum criterion provides a good initial estimation for the low-thrust ΔV required, it can be only applied to transfers with low eccentricity, [16]. As the eccentricity of the orbit used by the impulsive transfers cannot be known a priori, another additional constraint criterion was imposed in order to discard non-feasible solutions for the low-thrust transfer. In particular, a transfer was considered feasible only if:

$$ToF_{arc_k}\epsilon \geq C\Delta V_{arc_k}, \tag{7}$$

where ΔV_{arc_k} is the change in velocity required for the impulsive Lambert arc and C is an appropriate empirical coefficient.

If the considered Lambert arc meets all the above constraint criteria, then it is set as the new departure orbit ($\mathfrak{T}$), a new set of target asteroids $S_j = \{x : x \in S_{j-1} \wedge x \neq A_{Target_{j-1}}\}$ is initialized for the next transfer j, and all the previous steps are repeated. The process is repeated for all possible combinations of asteroids.

A full solution is generated when the local set of target asteroids S_j is empty, $S_j = \emptyset$ or if the end mission epoch has been reached. Given the number of visited asteroids N, the complete solution vector is as follow:

$$x = [\mathfrak{T}_1, T_1, ToF_1, A_1, \mathfrak{T}_2, T_2, ToF_2, A_2, \ldots, \mathfrak{T}_n, T_N, ToF_N, A_N], \tag{8}$$

where, for the first transfer, $\mathfrak{T}_1$ is the departure orbit, T_1 is the departure time, ToF_1 is the time of flight for the Lambert arc and A_1 is the target asteroid.

The main setting parameters of the LambTAN solver are summarized in Table 2.

Table 2. LambTAN parameters settings.

S	Target asteroids $[A_1, A_2, \ldots A_n]$
T_0	Mission start epoch
T_{end}	Mission end epoch
ToF_{max}	Maximum Time of Flight for each Lambert arc
ToF_{min}	Minimum Time of Flight for each Lambert arc
ToF_{step}	Time step for the Time of Flight
Δv_{MaxDep}	Maximum departure velocity
	$[\Delta v_{Earth}, \Delta v_{arc1}, \Delta v_{arc2}, ..., \Delta v_{arcn}]$
q_{min}	Minimum perihelion
ϵ	Low-thrust acceleration
C	Scaling factor

Additional Optimization

The optimization analysis previously described resulted in many solutions, each one characterized by a specific set of variables (number of asteroid visited, asteroid sequence, departure dates, time of flights). The solutions obtained were than ranked in order to identify the maximum sequence length and the lowest ΔV.

The best solutions obtained were further optimized by means of an evolutionary algorithm, Adaptive Inflationary Differential Evolution Algorithm, AIDEA [11]. AIDEA is an adaptive stochastic optimizer which combines Differential Evolution (DE), [12] with Monotonic Basin Hopping Algorithm (MBH) [13]. A brief description of the working mechanism of AIDEA is given in the following. AIDEA starts by initializing a population in the search space, starting from which the DE is run until the population contracts below a certain threshold. During the advancement from parents to offspring, the fundamentals parameters of the DE, crossover probability CR and differential weight F, [12], are automatically adapted. When the contraction condition is satisfied, a local search is performed from the best individual in the population to locate a local minimum and the population is restarted in a bubble around the detected local minimum. Local restart is iterated up to a predefined maximum value; when the maximum number of local restarts is reached the population is restarted globally, rather than locally, and the process resumes from the beginning. The algorithm stops when the maximum number of function evaluations is reached.

The optimization executed using AIDEA was done in order to identify better conditions for the departure dates. A given time window of ξ days was allocated around each departure date identified by the global optimization and AIDEA was run to find, in this interval, departure dates leading to a reduced value of the total ΔV. The arrival dates were fixed by the fly-by constraint to arrive at the asteroid when it is at its nodal point. The solutions obtained by the optimization process, and later refined using AIDEA, were used for the low-thrust trajectory optimization, described in the following subsection.

LOW-THRUST TRAJECTORY OPTIMIZATION

The aim of the low-thrust optimization was to determine the optimal control history for the spacecraft, using the optimized variables defined in the previous section. In particular, the low-thrust trajectory optimal control problem consisted in determining the control vector and parameters required to minimize the propellant consumption for the transfers.

Electric propulsion, while highly efficient, requires the engines to operate during a significant fraction of the trajectory and this makes it particularly difficult to find optimal trajectories [17]. The methods used to solve the continuous, low-thrust trajectory optimization problem generally fall into two categories: direct and indirect methods. Indirect methods are based on calculus of variations and on the formulation of a two-point boundary problem involving a set of costate variables, the solution of which yields a history of the time-dependent controls [18]. Finding a solution using indirect method is often difficult because of several reasons: the size of the dynamical system doubles in size when adding the costate variables, the convergence domain tends to be small and the problem is sensitive to the initial guesses of the costate variables, which are generally not physically intuitive [8]. Direct methods, on the other hand, are based on the parametrization of the controls and use nonlinear programming (NLP) techniques to optimize the performance index. Advantages of direct methods are the increased computational efficiency, more robust convergence and a reduced sensitivity to the initial guess, which is moreover physically more intuitive than for indirect methods [8]. Different methods are available to solve direct optimization method, e.g., single shooting, multiple shooting and collocation [18].

In this study, we considered a direct method and multiple shooting algorithm. In the multiple shooting algorithm, the trajectory is segmented into legs that begin and end at On/Off control nodes, where On nodes define the switching point from null thrust to maximum thrust and Off nodes define the switching point from maximum thrust to null thrust (Figure 3) [19]. The state vectors corresponding to each node are determined by the optimization process, being treated as optimizables controls [18]. The trajectory is therefore segmented into a sequence of thrust and coast legs. A middle point is defined for each transfer and the state vector is forward-propagated on each of the legs from the departure point to the mid point and back-propagated on each of the legs from the arrival point (that is, the asteroid nodal point) to the mid point.

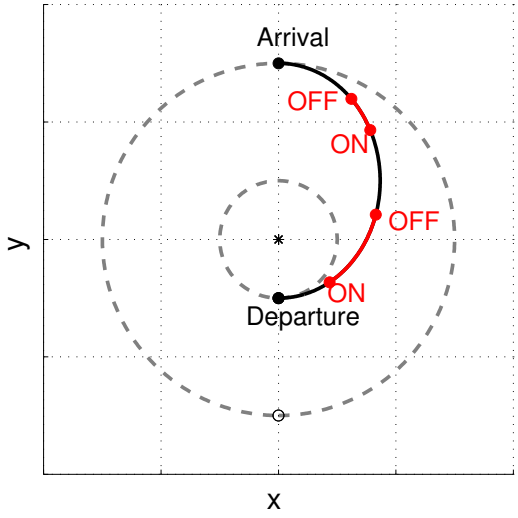

Figure 3. Segmentation of the trajectory into coast legs (black) and thrust legs (red).

Keplerian motion was considered on the coast legs, while on the thrust legs an analytical model for the propagation of the orbital motion under low thrust perturbation was used [20], [21]. Both indirect and direct methods tend to be computationally intensive when the trajectory is numerically integrated. However, the run time can be significantly reduced by using an analytic but accurate method like the one proposed in [21]. The perturbed two-body motion was expressed in terms of non-singular, equinoctial elements [22]:

$$\mathbf{X} = \begin{Bmatrix} a \\ P_1 \\ P_2 \\ Q_1 \\ Q_2 \\ L \end{Bmatrix} = \begin{Bmatrix} a \\ e\sin(\Omega+\omega) \\ e\cos(\Omega+\omega) \\ \tan(i/2)\sin\Omega \\ \tan(i/2)\cos\Omega \\ \Omega+\omega+f \end{Bmatrix}, \tag{9}$$

where f is the true anomaly. The equations of motion that are analytically integrated are expressed in terms of the Gauss planetary equations [23]. In these equations, the low-thrust perturbation is expressed in a radial-transversal reference frame, [20], as $\mathbf{u} = [u_r \quad u_t \quad u_h] = \epsilon\,[\cos\alpha\cos\beta \quad \sin\alpha\cos\beta \quad \sin\beta]$, where α, β, ϵ are, respectively, the azimuth, elevation and modulus of the acceleration; in particular $\epsilon = T/m$ where T is the engine thrust and m is the spacecraft mass. The equations of motion are completed considering that $dm/dt = -T/(I_{sp}g)$ where I_{sp} is the specific impulse of the low-thrust engine and g is the Earth sea-level gravitational acceleration. The engine acceleration ϵ is conservatively kept constant over each transfer and updated at the end of the transfer according to the mass consumption required for that transfer.

For the trajectory considered in this study, the angle β is always zero, since the transfers are all on the ecliptic plane. The azimuth angle α is instead an optimizable variable while the modulus ϵ of the acceleration depends on the mass of the spacecraft.

The optimization problem was therefore formulated as a non-linear programming problem whose objective is the minimization of the propellant consumption, subject to the following constraints:

- the state vector $\mathbf{X}$ at the termination of each leg (coast or thrust) should coincide with the state vector at the beginning of the next leg (thrust or coast);
- the time of flight should be equal to the required transfer time in order to reach the nodal point when the asteroid is there;

- the state vector over thrust and coast legs is propagated forward from the initial point up to a middle point and propagated backward from the final point to the middle point. A matching condition of the state vectors at the middle point is required.

Optimizable control variables are:

- thrust vector azimuth angle α;
- equinoctial elements at the beginning of each leg.

To obtain the solution of the non-linear programming problem, a continuation method [24] was implemented: an initial value of the acceleration greater than the nominal value was used to gradually obtain a solution with acceleration equal to the nominal value. At each step the initial guess for solution of the NLP problem was the the optimized vector obtained at the previous step (with a value of the acceleration greater than the current one).

VISIBILITY ANALYSIS

In the previous section, we presented a method to obtain an optimized trajectory to visit asteroids of the Atira group. During the transfer from one asteroid to another, observations of the inner part of the Solar System can be carried out with appropriate instrumentation placed on-board of the spacecraft, in order to potentially detect NEAs.

In this paper, the observations carried out throughout the mission lifetime were analysed from a statistical point of view [25]. We expect there to be a non-negligible number of undiscovered asteriods in the inner Solar System. Our analysis provides insight into the likelihood of observing members of this undetected population. Approximately 11,000 NEAs are currently known but the expected real number of NEAs is usually modeled using the cumulative distribution shown in Equation (10), [25]:

$$N(< H) = 10^{-3.88+0.39H}, \tag{10}$$

where H is the absolute magnitude of the asteroid and N is the number of NEAs with an absolute magnitude below H. We considered a total NEA population of 10^6 for the analysis presented in this paper.

First of all, the probability density and distribution functions of the absolute magnitude and orbital parameters of the NEAs population were obtained. The probability distributions of the absolute magnitude H, the semimajor axis a, the eccentricity e and the inclination i of the NEAs were computed using existing real data for the Minor Planet Center [7]. In addition, it was assumed that the ascending node, the argument of perihelion and the mean anomaly are uniformly distributed between 0 and 2π.

These functions were then included in the Monte Carlo simulation used to study the visibility throughout the low-thrust trajectory. The goal of these observations is to detect IEOs and therefore, the spacecraft's optical camera points towards the inner part of the orbit. The instrument that has been selected for the mission is the same one used for the Canadian microsatellite NEOSSat which was launched in 2003. This instrument has a limiting V magnitude of 19.5 with an exposure time of 100 seconds [26].

Probability Density and Distribution Functions

The probability density function of the absolute magnitude was computed by normalizing Equation (10) as follows:

$$\begin{aligned} f_H &= \frac{1}{C_H} \cdot 10^{-3.88+0.39H} \\ C_H &= \int_{H(N=1)}^{H(N=10^6)} 10^{-3.88+0.39H} dH \rightarrow f_H = 8.98\ 10^{-7} \cdot 10^{-3.88+0.39H} \end{aligned} \tag{11}$$

The probability distribution function has the form:

$$F_H = \int_{H(N=1)}^{H} 8.98\ 10^{-7} \cdot 10^{-3.88+0.39H} dH \tag{12}$$

The probability density and distribution functions for the inclination, semimajor axis and eccentricity of the orbit of the NEAs around the Sun were computed employing the existing data from the IAU Minor Planet Centre [7]. The data taken from the Minor Planet Centre were adjusted with polynomial functions for each parameter. Equations (13), (14) and (15) are the polynomial functions used for the semimajor axis, inclination and eccentricity respectively. In these equations N_a, N_e, N_i are the number of asteroids in each distribution.

$$\begin{aligned} N_a = -1555.8(a-0.5)(a-3.5) + 393.2a(a-0.5)(a-3.5), \\ a \in [0.5, 3.5]\text{AU}, \end{aligned} \tag{13}$$

$$\begin{aligned} N_e = 2523.4e \quad e \in [0, 0.55] \\ N_e = -15007e^3 + 44115e^2 - 43663e + 14553 \quad e \in [0.55, 1]. \end{aligned} \tag{14}$$

$$\begin{aligned} N_i = 0.25x + 0.144x^2 + 0.0072x^3 + 0.00013x^4, \\ x = i - 90, \ i \in [0, 90] \text{ deg}, \end{aligned} \tag{15}$$

The probability density functions were obtained by normalizing Equations (13), (14) and (15). The probability density functions of the three parameters are:

$$f_a = 0.114a^3 - 0.904a^2 + 1.996a - 0.786, \tag{16}$$

$$f_e = \begin{cases} 4.556e \quad e \in [0, 0.55] \\ -27.096e^3 + 79.654e^2 - 78.837e + 26.279 \quad e \in [0.55, 1] \end{cases}, \tag{17}$$

$$f_i = 1.92\ 10^{-9}\ i^4 - 5.84\ 10^{-7}\ i^3 + 6.63\ 10^{-5}\ i^2 - 0.003i + 0.06 \quad i \in [0, 90] \text{ deg}. \tag{18}$$

where f_a, f_e and f_i are the probability density functions of the semimajor axis, eccentricity and inclination. In addition, the probability distribution function can be computed as:

$$F_a = \int_{a=0.5}^{a} f_a da, \qquad F_e = \int_{e=0}^{e} f_e de \qquad F_i = \int_{i=0}^{i} f_i di. \tag{19}$$

Figure 4 shows the number of asteroids versus semimajor axis, eccentricity and inclination, as taken from the Minor Planet Center data and the probability distribution functions of a, e and i and H of the considered population. It can be observed that most of the NEAs are concentrated at low inclinations, semimajor axis close to 1.5 AU and eccentricities close to 0.5, which coincide with the results presented by Morbidelli et al. [27].

Observation Constraints

In order for the on-board camera to detect an asteroid, the following three constraints have to be met:

- the asteroid has to be within the Field of View (FOV) of the camera;
- the asteroid relative magnitude V with respect to the camera has to be below the camera detection threshold;
- the phase angle ϕ Sun-Asteroid-Spacecraft (Figure 5) has to be below a certain threshold.

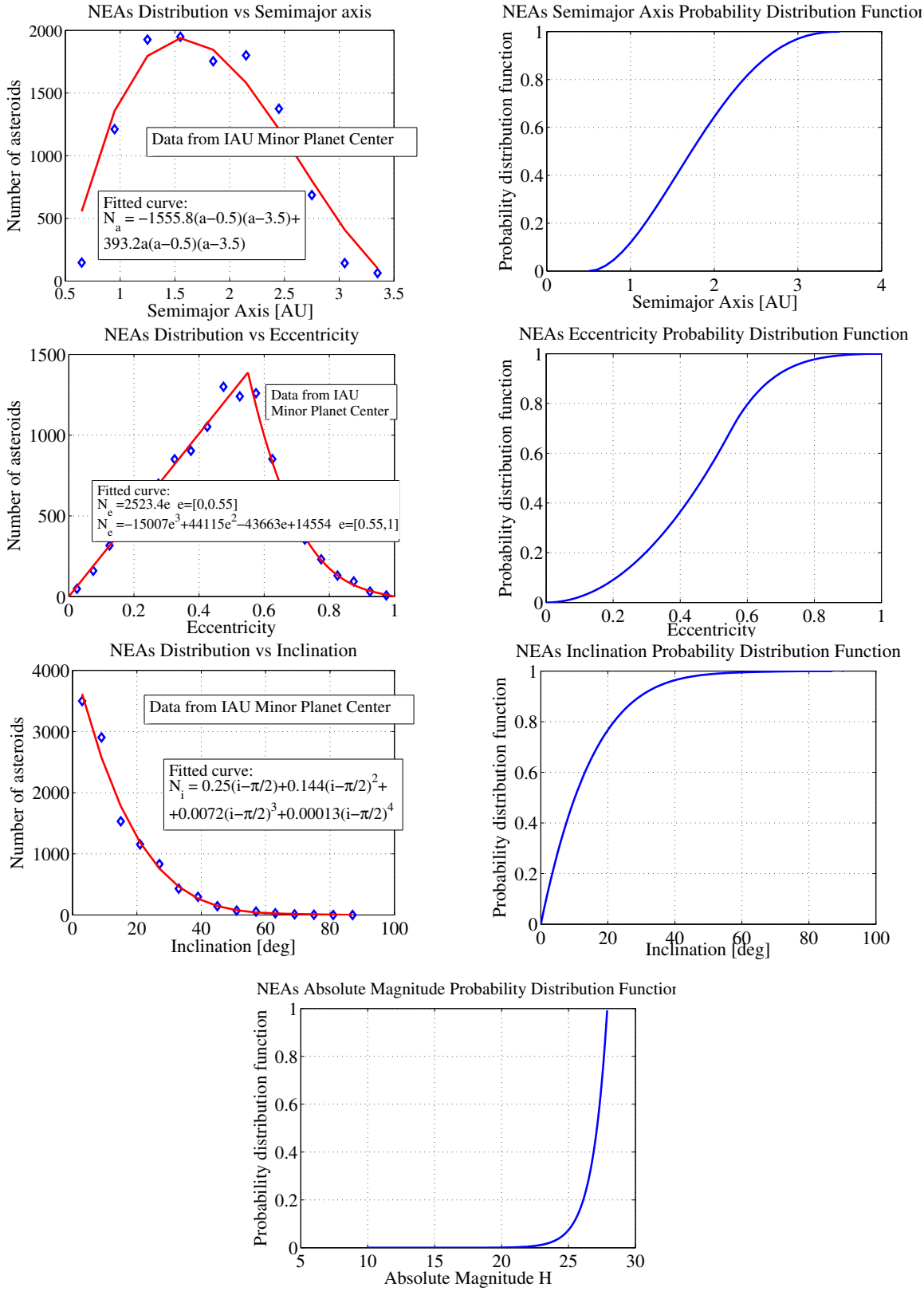

Figure 4. a, e **and** i **data from Minor Planet Centre and probability distribution functions of** a, e, i **and** H**.**

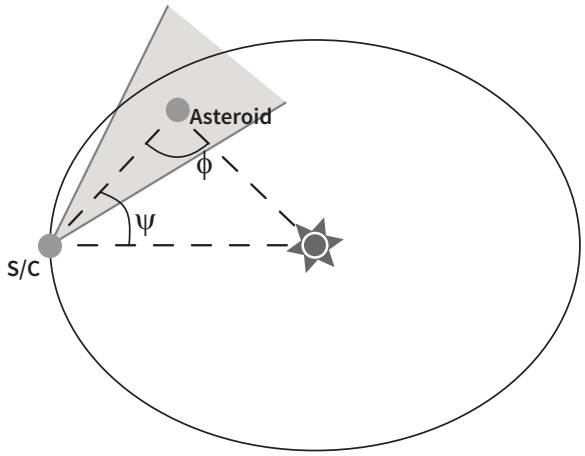

Figure 5. Camera pointing towards the inner part of the spacecraft trajectory.

The first two constraints are linked to the optical camera properties (FOV) and capabilities (limiting magnitude detection). The third constraint takes into account the necessary illumination conditions for the asteroid to be observed by the spacecraft. The best illumination conditions take place when $\phi = 0$. The asteroid relative magnitude V is given by [25]:

$$\begin{aligned} V &= 5\log_{10}(r\Delta) + H - 2.5\log_{10}((1-G)\lambda_1 + G\lambda_2), \\ \lambda_1 = \exp(-(3.33\tan(\frac{\phi}{2}))^{0.63}), &\qquad \lambda_2 = \exp(-(1.87\tan(\frac{\phi}{2}))^{1.22}), \end{aligned} \tag{20}$$

where H is the absolute magnitude of the asteroid, r is the distance between the asteroid and the Sun in AU, Δ is the distance between the asteroid and the spacecraft in AU, ϕ is the phase angle between the position vector between the asteroid and the Sun and the position vector between the asteroid and the spacecraft and G is the slope parameter of the asteroid. With these settings, the Monte Carlo simulation can be carried out during the optimized trajectory to study the possibility to observe new NEAs.

RESULTS

Sequence Finder

The parameters of the LambTAN solver were set as follow: the set of asteroids considered, S, is comprised of the first twelve asteroids from Table 1, the maximum mission time is 10 years, ΔV_{MaxDep} is 3 km/s from Earth and 1.5 km/s for the others departures, p_{min} is 46001200 km and ϵ is 10^{-4} m/s^2. All the simulation parameters are summarized in Table 3.

Table 3. LambTAN simulation parameters.

S	Asteroid 1 to 12 from Table 1
T_0	01/01/2020
T_{end}	01/01/2030
ToF_{max}	365 days
ToF_{min}	30 days
ToF_{step}	10 days
ΔV_{MaxDep}	3 km/s from Earth
	1.5 km/s from transfer orbits
q_{min}	0.31 AU
ϵ	10^{-4} m/s^2
C	2

The algorithm gave results in terms of optimal asteroid sequence and optimal departure and arrival dates. LambTAN was able to find 133761 solutions, with longest solutions characterized by six fly-bys; in Figure 6 the total ΔV required to realize all the solutions of four, five or six asteroids fly-bys are presented.

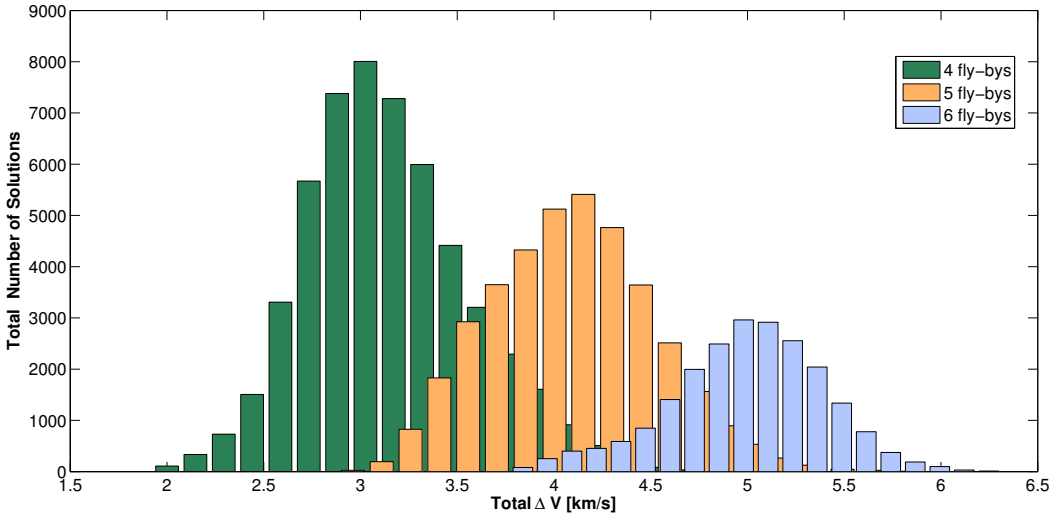

Figure 6. Solution distribution.

Since many of the solutions were characterized by the same sequences of asteroids but different departure and arrival dates, a filtering process was applied to identify solutions targeting different asteroids. The results of this filtering process demonstrated that the algorithm identified fourteen different solutions that visit six asteroids and fifty-seven solutions that visit five asteroids.

The best solution found by the LambTAN algorithm, that is, the one characterized by the maximum number of asteroid visited and the lowest total ΔV, has six fly-bys based on the following sequence: Earth - 2013JX28 - 2006WE4 - 2004JG6 - 2012VE46 - 2004XZ130 - 2008UL90 with a total ΔV cost of 3.77 km/s and a transfer time of about 8.4 years. If we consider a chemical propulsion specific impulse of $I_{sp} = 321$ s and a spacecraft dry mass of approximately 595 kg at the end of the six fly-bys (as found in Table 6), realizing the six fly-bys with a chemical engine would require 1377.36 kg of propellant. More details about this solutions are reported in Table 4. The positions of the targeted nodal points are shown in Figure 7 in the x - y plane of a heliocentric reference frame.

Table 4. Best solution obtained with six visited asteroids using LambTAN.

	Asteroid	Departure Date Lambert Arc	ToF Lambert Arc [days]	Arrival Date at Asteroid Node	ΔV [km/s]	Propellant mass [kg]
	2013JX28	2020/09/29	205	2021/04/22	0.87	476.54
	2006WE4	2022/05/14	215	2022/12/15	0.86	357.79
	2004JG6	2023/06/14	235	2024/02/04	0.61	200.60
	2012VE46	2024/09/11	265	2025/06/03	0.36	101.37
	2004XZ130	2026/09/15	205	2027/04/08	0.73	173.15
	2008UL90	2028/07/31	195	2029/02/11	0.34	67.91
TOTAL					3.77	1377.36

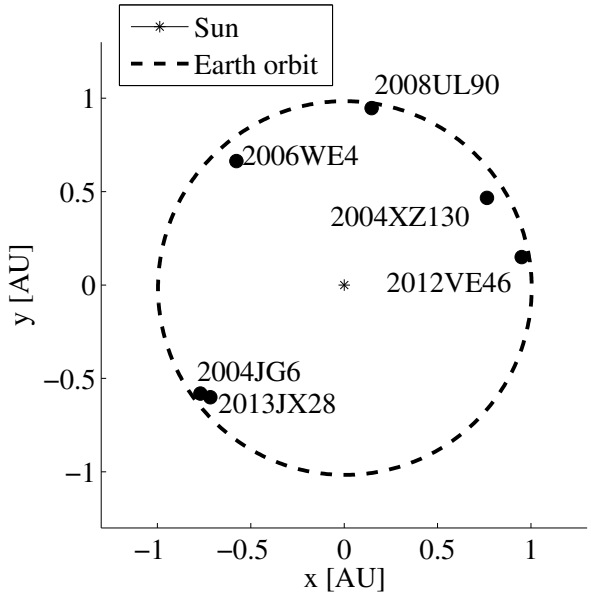

Figure 7. Targeted nodal points of the visited asteroids.

Refinement of the Best Solution

The best solution identified by LambTAN and presented in the previous section was further optimized using the global optimizer AIDEA. For the additional optimization a local window of $\xi = 10$ days was allocated around the previous defined departure dates in order to identify new departures dates leading to an improved result in term of total ΔV. The obtained results are reported in Table 5, showing a reduction of 0.16 km/s in the total ΔV and of 103.76 kg in the fuel consumption with respect to the results presented in Table 4.

Table 5. Further optimization of the best solution obtained with six visited asteroids using AIDEA.

	Asteroid	Departure Date Lambert Arc	ToF Lambert Arc [days]	Arrival Date at Asteroid Node	ΔV [km/s]	Propellant mass [kg]
	2013JX28	2020/09/20	214.5329	2021/04/22	0.95	487.06
	2006WE4	2022/05/24	205	2022/12/15	0.69	272.10
	2004JG6	2023/06/12	236.2514	2024/02/04	0.61	195.56
	2012VE46	2024/09/05	270.6114	2025/06/03	0.34	93.62
	2004XZ130	2026/09/18	201.5318	2027/04/08	0.72	167.80
	2008UL90	2028/08/10	185.0003	2029/02/11	0.29	57.46
TOTAL					3.61	1273.60

This solution and the results shown in Table 5 have been used for the optimization of the equivalent low-thrust trajectory.

Launch and Orbit Injection

The first transfer to the first asteroid in the sequence is realized through a hyperbolic escape from the Earth which injects the spacecraft directly into a heliocentric elliptic orbit that encounters the first asteroid at its nodal point. The spacecraft is initially placed on a Geostationary Transfer Orbit (GTO) characterized by the

following orbital elements [28]:

Altitude of perigee	$h_p = 250$ km
Altitude of apogee	$h_a = 36000$ km
Inclination	$i = 18$ deg
Argument of perigee	$\omega = 178$ deg

The heliocentric velocity of the spacecraft on its departure from Earth, $\mathbf{v}_{initial}$, is obtained from the solutions provided by the LambTAN algorithm. The relative velocity vector at the departure, $\mathbf{v}_\infty$, is obtained considering:

$$\mathbf{v}_\infty = \mathbf{v}_{initial} - \mathbf{v}_\oplus, \tag{21}$$

where $\mathbf{v}_\oplus$ is the velocity of the Earth expressed in the heliocentric reference frame [9]. The vector $\mathbf{v}_\infty$ is then transformed from heliocentric to planetocentric reference frame in order to obtain its declination δ, required to compute the inclination of the hyperbolic orbit according to [29]:

$$\sin i = \frac{\sin \delta}{\sin(\omega + \theta)}, \tag{22}$$

where θ is the true anomaly corresponding to the asymptotic direction [18] and ω is the perigee argument. For the considered transfer $\|\mathbf{v}_\infty\| = 0.65$ km/s and $\delta = -23.26$ deg. If a manouver to inject the spacecraft into the hyperbolic orbit was to be realized at the perigee of the GTO orbit, the following orbital parameter would be obtained for the hyperbolic orbit: $a = -9.41 \cdot 10^5$ km, $e = 1.01$ and $\theta = 173.22$ deg. However, for these values of θ, ω and δ, Equation (22) yields $\sin i > 1$, meaning that a change of i and ω is required to insert the spacecraft into the appropriate hyperbolic orbit. The values of i and ω corresponding to the lowest ΔV for the injection into the appropriate orbit are $\omega = 115$ deg and $i = 24.43$ deg. The inclination change is realized through a manoeuvre at the ascending node (close to the apogee of the GTO orbit) which requires $\Delta V = 0.18$ km/s while the perigee variation and injection into hyperbolic orbit requires $\Delta V = 0.91$ km/s, for a total velocity variation equal to $\Delta V = 1.09$ km/s. The two maneuvers are represented in Figure 8 in an Earth-centered reference frame (the GTO orbit is shown in blue, the GTO orbit after the inclination change is shown in red and the final hyperbolic orbit is in green).

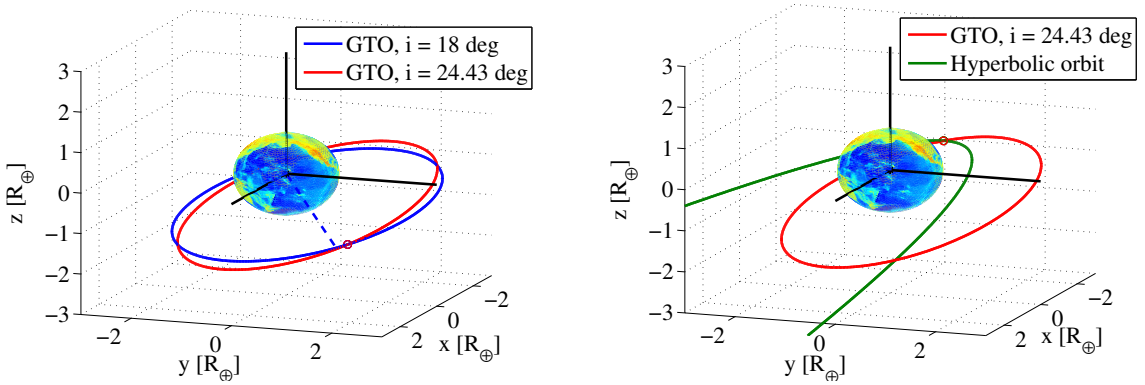

(a) First maneuver (b) Second manuever

Figure 8. Injection of the spacecraft into hyperbolic orbit: (a) variation of i of the GTO orbit; (b) variation of ω and insertion into hyperbolic orbit.

Considering a mass of the spacecraft of 700 kg and an upper stage characterized by a dry mass of 100 kg and an Isp of 321 s, the fuel required to inject the spacecraft into the hyperbolic orbit from the considered

GTO orbit is 331 kg and therefore the total mass to launch is:

$$m_{S/C} + m_{U/S} + m_{fuel} = (700 + 100 + 331)\text{ kg} = 1131\text{ kg}. \tag{23}$$

For this mass, a launch with the Indian Space Research Organisation PSLV-C4 (Polar Satellite Launch Vehicle) would be feasible [28].

Low-Thrust Trajectory Optimization

For the low-thrust optimization the initial acceleration was set at 10^{-4}m/s^2, equivalent to a thrust $T = 0.07$ N applied to a 700 kg spacecraft. The specific impulse considered was $I_{sp} = 3000$ s. The number of thrust legs for each transfer (from the departure point defined by the global optimization process to the asteroid nodal point) could vary between 2 and 8 and the initial acceleration for the continuation method could vary between 1 and 25 times the nominal acceleration.

Thanks to the strategy described in the previous section, the spacecraft is injected into an interplanetary orbit which allows it to realize the first fly-by without switching on the low-thrust engine. After the first fly-by the engine can be switched on to achieve the remaining five fly-bys. The results of the optimized low-thrust transfers are reported in Table 6.

Table 6. Summary of leg-by-leg simulation results for optimal, six-leg, low-thrust trajectory.

	Asteroid	Time Engine On [days]	m_0 [kg]	m_f [kg]	ΔV [km/s]
	2013JX28	0	700	700	-
	2006WE4	129.05	700	673.45	1.12
	2004JG6	152.57	673.45	642.07	1.37
	2012VE46	41.77	642.07	633.47	0.40
	2004XZ130	158.40	633.47	600.89	1.51
	2008UL90	30.04	600.89	594.17	0.30
TOTAL					4.70

After the last fly-by, the low-thrust engine is switched on again to execute the transfer to an orbit with lower perihelion (0.725 AU). This allows the spacecraft to move to inner regions of the Solar System to continue its observations of NEAs. Details of the transfer are given in Table 7.

Table 7. Summary of transfer to parking orbit after final fly-by for optimal, six-leg, low-thrust trajectory.

Departure Date	ToF [days]	Engine On [days]	Arrival Date	m_0 [kg]	m_f [kg]	ΔV [km/s]
2029/03/10	1135.6	192.31	2032/04/19	594.17	555.15	1.96

The total ΔV for the mission is:

$$\Delta V_{fly-by} + \Delta V_{parking-orbit} = (4.70 + 1.96)\text{ km/s} = 6.66\text{ km/s}. \tag{24}$$

The low-thrust engine enables the entire mission to be achieved with only approximately 145 kg of propellant, so that a spacecraft of 555 kg dry mass (Table 7) can be brought to the final parking orbit starting from a 700 kg spacecraft injected into orbit. This is a remarkable improvement over the propellant mass required for a chemical propulsion system (Table 5). The semimajor axis variation and the thrust angle profile during the trajectory are reported in Figure 9, together with a 0/1 flag representing the Off/On conditions of the engine. The fly-bys are indicated by the vertical lines. The spacecraft trajectory is represented in Figure 10 in the x - y plane of the heliocentric reference frame; the gray arcs are the coast legs and the black arcs are the thrust legs.

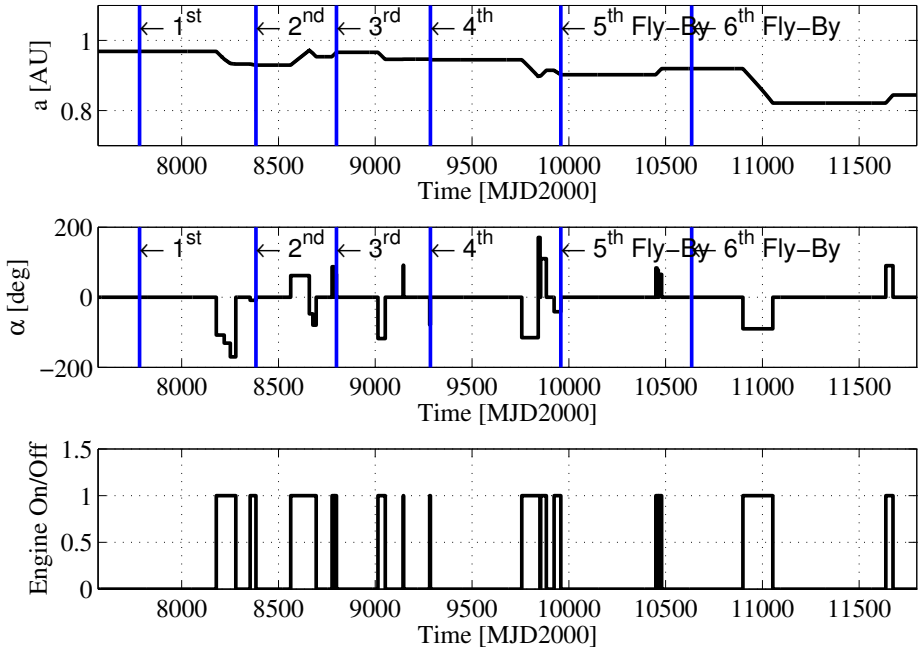

Figure 9. Semi-major axis (a), thrust angle (α), and switching function profiles for optimal, six-leg, low-thrust trajectory.

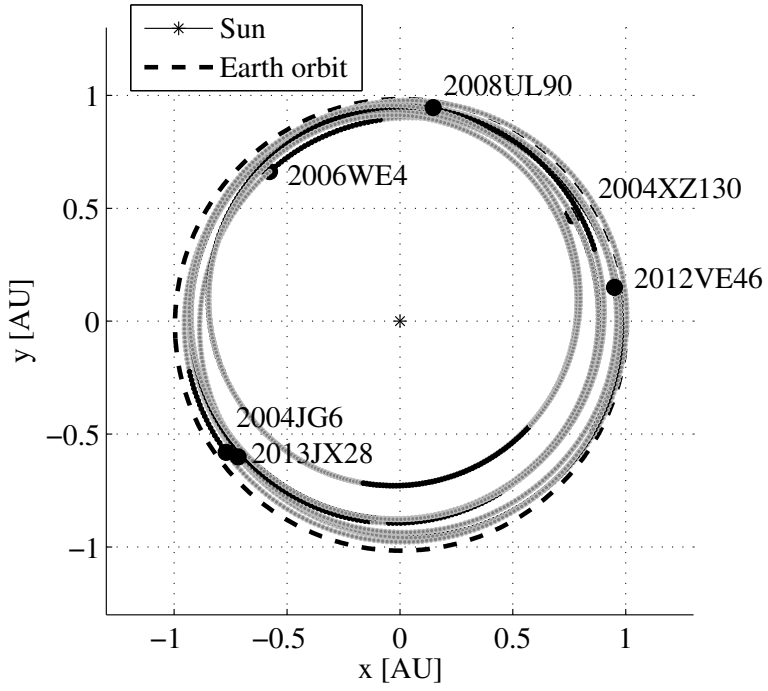

Figure 10. Best low-thrust solution trajectory. Thrust legs are in black and coast legs are in grey.

Visibility Analysis

A Monte Carlo simulation was carried out in order to study the visibility of undetected NEAs throughout the previously described low-thrust optimized trajectory. The constraints chosen for the observations are:

- observations are only carried out when the low-thrust engine is off;
- the angle ψ (angle Sun-spacecraft-Asteroid) is set to 45 degrees so that the camera does not point directly towards the Sun;
- the declination of the camera is zero degrees as the maximum population of asteroids is close to the ecliptic;
- the limiting magnitude of the camera is 19.5 and its FOV is 12 deg.

The diameter of the NEAs is related to the absolute magnitude as shown in Equation (25), [30],

$$D = \frac{1329}{\sqrt{p_v}} 10^{-0.2H}, \tag{25}$$

where D is the diameter in km, p_v is the albedo of the asteroid and H is the absolute magnitude.

For the simulations, a mean albedo of 0.14 was considered and the slope parameter G (Equation (20)) was set to its nominal value of 0.15 [25, 31]. Table 8 shows the results of the Monte Carlo analysis for each observation made by the spacecraft. As it was expected from the probability distribution functions, the mean value of the inclination is almost zero degrees, the mean value of the semimajor axis is close to 1.5 AU and the mean value of the eccentricity is close to 0.5. In addition, the mean size of the observed NEAs is 12 km. On average, 12 asteroids are detected during each observation, 3 of which are Atira asteroids (aphoelion Q lower than 0.983 AU). The total number of detected asteroids throughout the mission will depend on the number of observations that can be carried out.

Table 8. Mean values per observation for a maximum detection magnitude of 19.5.

Parameter	Mean Value	Min mean value	Max mean value	Standard deviation
Diameter [m]	12000	1.2	140000	$4 \cdot 10^{-14}$
Semimajor-Axis [AU]	1.43	0.7	2.6	0.11
Inclination [deg]	-0.0001	-0.1	0.1	0.01
Eccentricity	0.48	0.13	0.76	0.04
Total Observed Asteroids	12	–	–	3.25
Observed Atira Asteroids ($a < 1$ AU, $Q < 0.983$ AU)	3	–	–	1.9

CONCLUSIONS

This paper proposed a multiple-asteroid tour to visit the Atira asteroids using low-thrust propulsion while conducting observations of the inner region of the Solar System in order to possibly detect NEAs.

The initial domain-spanning optimization was solved considering impulsive transfer (Lambert problem implemented in LambTAN) for different departure dates and for arrival dates defined by the passing time of the asteroids at their nodal points. Due to the high computational complexity of the problem, the search space was pruned with plausible constraints. The solutions obtained were refined using a modified differential evolution algorithm. Using the departure dates, asteroid sequences and asteroid encounter epochs obtained from the optimization process, a low-thrust trajectory design optimization was run. The low-thrust optimization was solved using a direct method and multiple-shooting algorithm and an analytical model for the propagation of the spacecraft motion under low-thrust perturbation. A visibility analysis was conducted based on the optimal low-thrust trajectory computed to predict the number of asteroids that could be potentially discovered by the spacecraft using a dedicated camera. Results showed that six asteroids of the Atira group can be visited through fly-bys over a period of approximately 8.4 years. Furthermore, the final transfer to a parking orbit

with lower perihelion, which can increase the observation capability in the inner region of the Solar System, can be realized with a three-year extended mission. In addition, the ΔV required for the transfers resulted in limited propellant mass consumption, such that the mission can be conducted with a reasonably-sized spacecraft and limited launch mass. The visibility analysis showed that twelve asteroids can be detected as a mean value per observation, three of which belong to the Atira group, resulting in high scientific return for the spacecraft.

ACKNOWLEDGMENT

This work was partially supported by the Marie Curie Initial Training Network Stardust, FP7-PEOPLE-2012-ITN, Grant Agreement 317185 and by Airbus Defence and Space.

REFERENCES

[1] JPL Small-Body Database Search Engine - ssd.jpl.nasa.gov/sbdb-query.cgi.

[2] M. D. Rayman and S. N. Williams, "Design of the First Interplanetary Solar Electric Propulsion Mission," Journal of Spacecraft and Rockets, Vol. 39, No. 4, July-August 2002, pp. 589–595.

[3] J. Kawaguchi, "The Hayabusa Mission - its seven years flight," 2011 Symposium on VLSI Circuits, Honolulu, HI, 15-17 June 2011.

[4] M. D. John R. Brophy and B. Pavri, "Dawn: An Ion-Propelled Journey to the Beginning of the Solar System," IEEE Aerospace Conference, Big Sky, MT, March 2008.

[5] S. N. Williams and V. Coverstone-Carroll, "Benefits of Solar Electric Propulsion for the Next Generation of Planetary Exploration Missions," The Journal of the Astronautical Sciences, Vol. 45, No. 2, April-June 1997, pp. 143–159.

[6] C. G. Sauer and C.-W. Yen, "Planetary Mission Capability of Small Low Power Solar Electric Propulsion System," IAA International Conference on Low-Cost Planetary Missions, Laurel, MD, 12-15 April 1994.

[7] "Minor Planet Center," The International Astronomical Union (IAU) - http://www.minorplanetcenter.net/iau/mpc.html, 2013.

[8] K. Alemany and R. D. Braun, "Survey of Global Optimization Methods for Low-Thrust, Multiple Asteroid Tour Mission," AAS/AIAA Space Flight Mechanics Meeting, AAS 07-211, Sedona, Arizona, 28 January - 1 February 2007.

[9] D. A. Vallado, Fundamentals of Astrodynamics and Applications. Space Technology Library, 2001.

[10] D. D. M. Roger R. Bate and J. E. White, Fundamentals of Astrodynamics. Dover Books on Aeronautical Engineering, 1972.

[11] M. Vasile and E. Minisci, "Adaptive Inflationary Differential Evolution Algorithm," 2014 IEEE Congress on Evolutionary Computation (CEC), Beijing, 06-11 July 2014, pp. 1792–1799.

[12] K. Price, R. M. Storn, and J. A. Lampinen, Differential Evolution. A Practical Approach to Global Optimization. Natural Computing Series, Springer, 2005.

[13] D. J. Wales and J. P. K. Doye, "Global Optimization by Basin-Hopping and the Lowest Energy Structures of Lennard-Jones Clusters Containing up to 110 Atoms," Journal of Physical Chemistry, Vol. 101, No. 28, 1997, pp. 5111–5116.

[14] D. R. M. Victor M. Becerra, S. J. Nasuto, M. J. Bishop, and D. Izzo, "An efficient pruning technique for the global optimisation of multiple gravity assist trajectories," International Workshop on Global Optimization, San Jos, Almera, Spain, 13-17 June, 2005.

[15] D. Novak and M. Vasile, "Incremental Solution of LTMGA Transfers Transcribed with and Advanced Shaping Approach," International Astronautical Congress, Prague, 27 September - 01 October 2010.

[16] V. A. Chobotov, Orbital Mechanics. AIAA Education Series, 2002.

[17] J. A. Sims and S. N. Flanagan, "Preliminary Design of Low-Thrust Interplanetary Missions," AAS/AIAA Astrodynamics Specialist Conference, AAS 99-338, Girdwood, Alaska, 21-24 August 2006.

[18] S. Kemble, Interplanetary Mission Analysis and Design. Springer Praxis Book, 2006.

[19] C. H. Yam and J. M. Longuski, "Reduced Parametrization for Optimization of Low-Thrust Gravity-Assist Trajectories: Case Studies," AAS/AIAA Astrodynamics Specialist Conference and Exhibition, AIAA 2006-6744, Keystone, CO, 21-24 August 2006.

[20] M. V. Federico Zuiani, A. Palmas, and G. Avanzini, "Direct Transcription of Low-Thrust Trajectories with Finite Trajectory Elements," Acta Astronautica, Vol. 72, 2012, pp. 108–120.

[21] F. Zuiani and M. Vasile, "Extended analytical formulas for the perturbed Keplerian motion under a constant control acceleration," Celestial Mechanics and Dynamical Astronomy, 2014, 10.1007/s10569-014-9600-5, pp. 1–26.

[22] R. Broucke and P. Cefola, "On the Equinoctial Orbit Elements," Celestial Mechanics, Vol. 5, No. 3, 1972, pp. 303–310.

[23] R. H. Battin, Introduction to the Mathematics and Methods of Astrodynamics. AIAA Educational Series, 1987.

[24] B. Bonnard, L. Faubourg, and E. Trélat, Mećanique céleste et contrôle des véhicules spatiaux, Vol. 51. Springer, 2006.

[25] J. S. Stuart, Observational constraints on the number, albedos, sizes and impact hazards of the near-earth asteroids. PhD thesis, Massachusetts Institute of Technology, 2003.

[26] B. Wallace, R. L. Scott, M. Sale, A. Hildebrand, and R. Cardinal, "The Near Earth Object Surveillance Satellite: Mission status and CCD evolution after 18 months on-orbit," Advanced Maui Optical and Space Survaillance Technologies Conference (AMOS), Maui, Hawaii, 09-12 September 2014.

[27] A. Morbidelli, F. W. Bottke, C. Froeschle, and P. Michel, "Origin and Evolution of Near-Earth Object," Asteroids III, University of Arizona Press, 2002, pp. 409–422.

[28] Indian Space Research Organisation - http://www.isro.org/pslv-c4/pslv-c4.aspx.

[29] K. Sorensen, "Hyperbolic Injection Issues for MXER Tethers," 39th AIAA/ASME/SAE/ASEE Joint Propulsion Conference, 21-23 July 2003.

[30] E. F. Tedesco, G. J. Veeder, J. W. Fowler, and J. R. Chillemi, "The IRAS Minor Planet Survey," Tech. Rep. AD-A276726, Phillips Laboratory. Directorate of Geophysics, December 1992.

[31] A. Harris, "NEA populations and impact frequency," NASA Asteroid Grand Challenge Seminar, March 2014.